Mechanical Systems and Signal Processing 98 (2018) 352–367

Contents lists available at ScienceDirect

Mechanical Systems and Signal Processing

journal homepage: www.elsevier.com/locate/ymssp

Statistical analysis of modal parameters of a suspension bridge based on Bayesian spectral density approach and SHM data

Zhijun Li [a,*], Maria Q. Feng [b], Longxi Luo [b], Dongming Feng [b], Xiuli Xu [a]

[a] College of Civil Engineering, Nanjing Tech University, Nanjing 211800, China
[b] Department of Civil Engineering and Engineering Mechanics, Columbia University, New York, NY 10027, United States

ARTICLE INFO

Article history:
Received 9 September 2016
Received in revised form 3 March 2017
Accepted 7 May 2017
Available online 16 May 2017

Keywords:
System identification
Bayesian spectral density method
Suspension bridge
Structural health monitoring system
Statistical distribution
Temperature
Wind

ABSTRACT

Uncertainty of modal parameters estimation appear in structural health monitoring (SHM) practice of civil engineering to quite some significant extent due to environmental influences and modeling errors. Reasonable methodologies are needed for processing the uncertainty. Bayesian inference can provide a promising and feasible identification solution for the purpose of SHM. However, there are relatively few researches on the application of Bayesian spectral method in the modal identification using SHM data sets. To extract modal parameters from large data sets collected by SHM system, the Bayesian spectral density algorithm was applied to address the uncertainty of mode extraction from output-only response of a long-span suspension bridge. The posterior most possible values of modal parameters and their uncertainties were estimated through Bayesian inference. A long-term variation and statistical analysis was performed using the sensor data sets collected from the SHM system of the suspension bridge over a one-year period. The t location-scale distribution was shown to be a better candidate function for frequencies of lower modes. On the other hand, the burr distribution provided the best fitting to the higher modes which are sensitive to the temperature. In addition, wind-induced variation of modal parameters was also investigated. It was observed that both the damping ratios and modal forces increased during the period of typhoon excitations. Meanwhile, the modal damping ratios exhibit significant correlation with the spectral intensities of the corresponding modal forces.

1. Introduction

Vibration-based structural health monitoring (SHM) techniques have become valuable methods for evaluating structural integrity, and reliability throughout the life-cycle of structures. The SHM techniques are often based on modal parameters such as natural frequencies, damping ratios and mode shapes [1]. However, in field conditions, when structures are subject to changing environmental conditions, the modal parameters of the structure exhibit non-stationary behavior [2–4]. Meanwhile, since the ambient vibration and operational conditions such as wind and traffic may affect the measured signals, the identified modal parameters will exhibit uncertainties. Therefore, the modal parameters identification methods need to provide estimation of the parameter uncertainty.

* Corresponding author.
E-mail address: lizhijun@njtech.edu.cn (Z. Li).

http://dx.doi.org/10.1016/j.ymssp.2017.05.005
0888-3270/

During the past few decades, modal identification of civil engineering structures based on ambient vibration measurements has been widely investigated, and a variety of output-only modal identification methods have become available in both time and frequency domains [5]. Among the frequency domain methods, the peak picking (PP) and frequency-domain decomposition (FDD) techniques are most widely used [6]. Although many methods are available in literature for identification of modal parameters, there are relatively few studies on the statistical bounds of the identified parameters [7]. While time domain methods have some advantages in identifying the closed modes and damping ratios, they have some drawbacks. The advantage of stochastic subspace identification (SSI) methods is that they are numerically robust and non-iterative. However, most of SSI algorithms do not provide any direct estimation of the variance of the identified modal parameters [7].

Bayesian inference provides a promising and feasible identification solution for the purpose of structural health monitoring. The Bayesian approaches offer a powerful tool for system identification that explicitly addresses uncertainty. A significant advantage of the Bayesian inference is that not only the optimal estimates can be determined but also their associated uncertainties can be quantified in the form of probability distributions [8]. Recently, there is a rising interest in computing the uncertainties of modal parameters using the Bayesian approaches including the Bayesian spectral density approach (BSDA) [9], Bayesian time domain approach, and Bayesian FFT approach [10–12]. These methods provide rigorous means for obtaining modal properties as well as their uncertainties for given measured data and modeling assumptions. Although there exist many Bayesian approaches, computational difficulty has severely hindered their wider applications. In [11], a two-stage fast Bayesian Spectral Trace Analysis (BSTA) method is developed, which can address the computational challenges of the conventional Bayesian approach. In the BSTA method, the interaction between the spectrum variables (i.e., frequency, damping ratio as well as the spectral density of modal excitation and prediction error) and the spatial variables (i.e., mode shape components) can be decoupled completely. Although the theory and computational methods provide a rigorous and viable platform, practical and important issues regarding data limitation, interpretation of results, trade-off between identification precision and modeling error risk need to be addressed for application of the Bayesian spectral density approach in real structures [13].

In the case of bridges, environmental factors such as temperature, wind profile and traffic are known to increase the variance of a modal frequency. The influence of varying environmental conditions on structural modal properties has been extensively investigated through field measurements and dynamic tests [14–17]. Results from monitoring of the Humber Bridge showed that the temperature and the wind were the two most significant influences on the bridge behavior [18]. Several studies have shown that operational modal parameters obtained using vibration-based structural monitoring systems are not fixed and can vary within 5% of their range from their mean value [2,15]. However, the relationships between the modal frequencies and the environmental and loading effects (e.g. temperature, wind, traffic) are complex. In [19], it was observed that the dynamic behavior of the suspension bridges is dependent on the magnitude of the environmental effects. For instance, the fundamental frequency of a suspension bridge reduces as the wind speed increases. On the other hand, the modal damping increases when the wind velocity increases and exceeds a certain level. According to long term observation and estimation results of the operational modal parameters, the uncertainty distributions of these parameters can be fitted by normal distributions [20]. Although a lot of field measurements and observations were conducted regarding the relation between the modal frequency and the environmental influences, very few studies addressed the statistical distribution over a long period time. Moreover, the variation of damping parameters was rarely studied.

This paper presents a statistical analysis for the modal parameters of the Runyang Suspension Bridge (RSB) based on its SHM data. RSB is a long-span suspension bridge constructed in 2005 over Yangtze River, China. Since 2005, a long-term structural monitoring system installed on the bridge provides large data sets. As there are a large amount of data sets recorded by the SHM system of the bridge, a robust and automatic identification method is necessary. To process large data sets for the long-term structural monitoring system, the Bayesian spectral density algorithm is adapted to address the uncertainty of modes extraction from output-only response. Furthermore, the extraction of modal parameters is fully automated by introduced the Bayesian spectral trace analysis method, which can address the computational difficulties of conventional BSDA. Moreover, statistical studies of the operational modal parameters over a long-term period were conducted to study the parameter distributions and variation. In addition, a period data sets during a strong wind excitation is presented to research the wind-induced variation of modal parameters.

2. Bayesian spectral density approach for output-only modal identification

2.1. Dynamics of linear systems

Consider a linear dynamic system with N_d degrees of freedom and equation of motion:

$$\boldsymbol{M}\ddot{x}(t) + \boldsymbol{C}\dot{x}(t) + \boldsymbol{K}x(t) = \boldsymbol{T_0}\boldsymbol{W}(t) \tag{1}$$

where $\boldsymbol{M}$, $\boldsymbol{C}$ and $\boldsymbol{K}$ are the mass, damping and stiffness matrix, respectively; $\boldsymbol{T}_0$ is a force distributing matrix. The external excitation $\boldsymbol{W}$ can be modeled as zero-mean Gaussian white noise with spectral intensity matrix $\boldsymbol{S_W}(\omega) = \boldsymbol{S_{W0}}$.

Using modal analysis, one obtains the uncoupled modal equations of motion:

$$\ddot{\boldsymbol{q}}_{r(t)} + 2\xi_r\omega_r\dot{\boldsymbol{q}}_{\boldsymbol{r}}(t) + \omega_r^2\boldsymbol{q}_{\boldsymbol{r}}(t) = \boldsymbol{w}_{\boldsymbol{r}}(t), \quad r = 1, \ldots, N_d \tag{2}$$

where $\omega_r = 2\pi f_r$; f_r, ξ_r, $q(t)$ and $w(t)$ are the natural frequency (in Hz), damping ratio, the modal co-ordinate vector and the modal forcing vector respectively. The transformation between the original co-ordinates and the modal co-ordinates is given by

$$\boldsymbol{x}(t) = \boldsymbol{\psi} \cdot \boldsymbol{q}(t) \tag{3a}$$

$$\boldsymbol{w}(t) = \boldsymbol{\psi}^T \cdot \boldsymbol{W}(t) \tag{3b}$$

where $\boldsymbol{\Psi}$ is the mode shape matrix. The columns of the mode shape matrix are the mode shape vectors $\boldsymbol{\psi}^{(r)},\ r = 1,\ldots,N_d$.

Assume that the measurement $\boldsymbol{y_N} = \{\boldsymbol{y}(n),\ n = 1,2\ldots,N\}$ contains N_0 channels of structural response, corrupted by the measurement noise $\mu(n)$

$$\boldsymbol{y}(n) = \boldsymbol{L_0 x}(n) + \boldsymbol{\mu}(n) \tag{4}$$

where $\boldsymbol{y}(n) \in \mathbb{R}^{N_0}$ is the measurement at the *nth* time step; $\boldsymbol{L_0 x}(\boldsymbol{n})$ is the concerned structural response (e.g., displacement or acceleration) at the same time step, where $\boldsymbol{L}_0$ denotes an $N_0 \times N_d$ observation matrix, comprised of zeros and ones. Herein, the measurement noise is modeled as zero-mean Gaussian white noise process vector $\boldsymbol{\mu}(n)\mathbb{R}^{N_0}$, which satisfies

$$E[\boldsymbol{\mu}(\boldsymbol{n})\boldsymbol{\mu}^T(\rho)] = \sum_{\boldsymbol{\mu}} \delta_{n\rho} \tag{5}$$

where $E[\cdot]$ denotes expectations, $\delta_{n\rho}$ denotes the Kronecker delta function, and $\sum_{\boldsymbol{\mu}}$ denotes the $N_0 \times N_0$ covariance matrix of the prediction error process $\boldsymbol{\mu}$. The covariance matrix $\sum_{\boldsymbol{\mu}}$ is often diagonal and often assumed to be of the form $s_{\boldsymbol{\mu}}\boldsymbol{I}_{N_0}$

Let λ denote the full set of modal parameters to be identified. It consists of the modal frequencies f_r and damping ratios ξ_r of the concerned modes, the partial mode shapes $\psi(r)$ including only the components at the observed degrees of freedom of the concerned modes, the upper triangles (diagonal inclusive) of $\boldsymbol{S_w}$ and the modeling error $s_{\boldsymbol{\mu}}$.

$$\lambda = \left[\{f_r, \xi_r\};\ \boldsymbol{S}_{\boldsymbol{w},rr'} : r, r' = 1,\ldots,n_r;\ r' < r\};\ s_{\boldsymbol{\mu}};\ \{\psi^{(r)}\}\right] \tag{6}$$

2.2. Statistical characteristics of response power spectral density

To identify the uncertain modal parameter vector λ, a discrete estimator of the power spectral density matrix is utilized [9].

$$\boldsymbol{S}_{Y,N}(k) = \boldsymbol{Y}_N(k)\boldsymbol{Y}_N^*(k) \tag{7}$$

where the asterisk '$*$' denotes a complex conjugate transpose. $\boldsymbol{S}_{\boldsymbol{Y},N}(k)$ is an N sample based estimate of the power spectral density and it is a random variable. And $\boldsymbol{Y}_N(k)$ is defined as the Fourier transform of the vector process at frequency f_k

$$\boldsymbol{Y}_N(k) = \sqrt{\frac{\Delta t}{2\pi N}} \sum_{m=0}^{N-1} \boldsymbol{y}(m) e^{-i2\pi f_k m\Delta t} \tag{8}$$

where $i^2 = -1$, $f_k = k\Delta f,\ k = 0,\ldots,N_l - 1$ with $N_l = INT\left(\frac{N}{2}\right)$, $\Delta f = 1/T$, and $T = N\Delta t$. INT stand for the integer part.

It has been proved in [21] that the random vector $\boldsymbol{Y}_N(k)$ follows a Gaussian distribution as $N \to \infty$. Assume now that there is a set of independent time histories $\boldsymbol{y}_N^{(1)},\ldots,\boldsymbol{y}_N^{(n_s)}$ with the same distribution function. The corresponding Fourier transforms $\boldsymbol{Y}_N^j(k),\ j = 1,\ldots,n_s$ are independent and follow an identical complex N_0-variate normal distribution with zero mean. Then the sum of spectral density matrix estimator

$$\boldsymbol{S}_k^{sum} = \sum_{j=1}^{n_s} \boldsymbol{Y}_N^j(k)\boldsymbol{Y}_N^{j^*}(k) \tag{9}$$

follows the central complex Wishart distribution of dimension n_0 with n_s degrees of freedom.

2.3. Bayesian spectral trace approach(BSTA)

In [11], a Bayesian spectral trace approach was proposed by collecting the auto-spectral densities. It is assumed that the spectral density set $\boldsymbol{S}_{\wp}^{sum} = \{\boldsymbol{S}_k^{sum},\ k = k_1,\ldots,k_2\}$ formed over the frequency band $\wp \in [k_1\Delta f, k_2\Delta f]$ is employed for ambient modal analysis.

According to the Bayes' theorem, the posterior probability density function (PDF) of $\boldsymbol{\lambda}$ given $tr(\boldsymbol{S}_{\wp}^{sum})$ is

$$p\left(\boldsymbol{\lambda}|tr\left(\boldsymbol{S}_{\wp}^{sum}\right)\right) = c_1 p(\boldsymbol{\lambda}) p\left(tr(\boldsymbol{S}_{\wp}^{sum}|\boldsymbol{\lambda})\right) \tag{10}$$

Assuming a uniform (constant) prior distribution is used for $\boldsymbol{\lambda}$, the optimal modal parameter vector $\hat{\boldsymbol{\lambda}}$ can be obtained by minimizing the objective function defined as $L_{BSTA}(\boldsymbol{\lambda}) = -ln^{p\left(tr(\boldsymbol{S}_p^{sum}|\boldsymbol{\lambda})\right)}$. It is convenient to write the objective function in terms of the 'negative log-likelihood function' (NLLF) as

$$L_{BSTA}(\boldsymbol{\lambda}) = \frac{1}{2}\sum_{k=k_1}^{k_2} \ln\left[2\pi n_s tr(\Re(C_k^2(\boldsymbol{\lambda})))\right] + \sum_{k=k_1}^{k_2} \frac{\left[tr(\boldsymbol{S}_k^{sum}) - n_s tr(\boldsymbol{C}_k(\boldsymbol{\lambda}))\right]^2}{2n_s tr(\Re(\boldsymbol{C}_k^2(\boldsymbol{\lambda})))} \tag{11}$$

In the aforementioned function, $\Re(\cdot)$ denotes the real part of a complex number. For the case of separated modes, there is only one mode to be identified for a specified frequency band, i.e. $\boldsymbol{\lambda} = \{f_s, \xi_s, s_{ws}, s_{\mu s}, \boldsymbol{\psi}_S\}$. The NLLF of BSTA is given by

$$L_{BSTA}(\boldsymbol{\lambda}) = \frac{1}{2}\sum_{k=k_1}^{k_2} \ln\left[2\pi n_s\left(\Lambda_k^2 + 2s_{\mu s}\Lambda_k + n_0 s_{\mu s}^2\right)\right] + \sum_{k=k_1}^{k_2} \frac{\left[tr(S_k^{sum}) - n_s(\Lambda_k + n_0 s_{\mu s})\right]^2}{2n_s\left(\Lambda_k^2 + 2s_{\mu s}\Lambda_k + n_0 s_{\mu s}^2\right)} \tag{12}$$

From (12), the NLLF can be obtained by constrained numerical optimization without much computational effort, which can be done by using the function 'fminsearch' in MATLAB.

To identify the mode shape, it has also been proved in [11] that the optimal mode shape $\hat{\psi}_s$ can be obtained by performing a singular value decomposition on $\boldsymbol{\Xi}$ after substituting optimal $\hat{f}_s$, $\hat{\xi}_s$, $\hat{S}_{ws}$ and $\hat{s}_{\mu s}$ into (13).

$$\boldsymbol{\Xi} = \sum_{k=k_1}^{k_2}\left[1 + \left(s_{\mu s}/\Lambda_k\right)\right]^{-1}\boldsymbol{S}_k^{sum} \tag{13}$$

2.4. Posterior uncertainty of spectrum variables

The most probable parameter vector $\hat{\lambda}$ can be obtained by minimizing $L_{BSTA}(\boldsymbol{\lambda})$, while the covariance matrix of the modal parameters can be obtained by taking the inverse of the Hessian of $L_{BSTA}(\boldsymbol{\lambda})$ evaluated at $\boldsymbol{\lambda} = \hat{\boldsymbol{\lambda}}$, i.e., $\sum_{\lambda} = \left[\Gamma(\hat{\boldsymbol{\lambda}})\right]^{-1}$ .The elements of $\Gamma(\hat{\boldsymbol{\lambda}})$ can be calculated either analytically as shown in [11] or using finite difference approach.

3. Application of Bayesian spectral method in SHM of RSB

3.1. Description of Runyang suspension bridge

The Runyang Suspension Bridge, as shown in Fig. 1, is one of the most critical traffic links spanning the Yangtze River, China. At the time of its completion in 2005, it was the longest suspension bridge in China. RSB consists of a 1490 m main span and two 470 m side spans. The cross section of the deck of RSB is an aerodynamically shaped closed steel box girder, which carries two carriageways and three traffic lanes on each carriageway. The width and the height of the steel box girder are 36.3 m and 3.0 m respectively. The main cable is composed of parallel subsection cables. The main span is supported by two towers, each one of which is approximately 210 m tall. Each of the two concrete towers (the south tower in Zhenjiang side and the north tower in Yangzhou side) is composed of two reinforced concrete columns connected by three horizontal prestressed cross-beams at different levels.

Fig. 1. View of the Runyang Suspension Bridge.

3.2. Introduction of the SHM system of RSB

After the completion of the RSB Bridge in 2005, a permanent SHM system was installed and has been continuously conducting real-time bridge response measurements [22]. The system consists of a wide range of analog sensors, including accelerometers, anemometers, strain gauges, displacement sensors, temperature sensors and global position system (GPS). Sixty-five uniaxial accelerometers were used to measure the vibration of the bridge. The accelerometer layout of the SHM system is shown in Fig. 2, with 8 lateral accelerometers and 4 vertical accelerometers on the four sections of the main cable, 29 accelerometers on the nine sections of the main-span bridge deck, and 12 accelerometers installed on the north and south tower, respectively. Thus, there are a total of 65 accelerometers. All accelerometers are Kistler K8330A and K8310A, which have a sensitivity of 1.5 V/g with 2.5 μg resolution. The accelerometer signals are amplified by a gain of 100 before streaming into the digitizer at a sampling frequency of 20 Hz. In the frequency range of interest (0.05–1 Hz), the overall channel noise is about a few $\mu g/\sqrt{Hz}$.

In this study, the accelerometers along the bridge deck are primarily used to identify modal properties of RSB using output-only system identification method.

3.3. Modal parameter identification using the BSTA

System identification of RSB using the BSTA is carried out based on the SHM system data sets. Figs. 3 and 4 show the typical power spectral densities (PSD) at different sections calculated using the vertical responses of the deck. The duration and the sampling time interval of each set are 1638 s and 0.05 s, respectively. The resolution in the modal frequency identification can be calculated using the function below

$$\Delta f = \frac{fs}{NFFT}$$

where fs = sampling frequency and $NFFT$ = number of FFT points. When fs = 20 Hz and $NFFT$ = 1024×32 = 32,768, the resolution in the modal frequency can be obtained as 6.1×10^{-4} Hz.

To identify the vertical modal parameters, 6 channels of vibration response of the deck with high signal-noise ratio were used, which were obtained from the 1/8 section, 3/8 to 7/8 section of the bridge respectively. Since the BSTA method requires the number of available data sets to be larger or equal to the number of measured DOFs ($M \geqslant N_s$), 6 sets (M = 6) of response history are considered. Fig. 5 shows the trace of PDF of the girder vertical response, i.e. $tr(\boldsymbol{S}_k^{sum})$, estimated using 6 sets of samples. The subset frequency in the range of $[0.8f_m, 1.2f_m]$ was used for calculating the posterior PDF of the parameters. It was found that the uncertainties of the modal frequency and damping ratio remain almost unchanged when the frequency range increases, implying that most of the information regarding these two parameters are contained in the frequency range around the target modal frequency [9].

3.4. Discrimination of vertical bending and torsional modes

From Fig. 5, it can be seen that most of the modes could be well separated in the frequency range from 0 Hz to 0.6 Hz. However, an analysis result based on the stochastic subspace identification (SSI) method, illustrated in Fig. 6, indicated that there were two adjacent modes close to each other near the frequency of 0.24 HZ, which includes a vertical mode (V5) and a first symmetric torsional mode (T1).

To separate the bending signal of V5 and torsional signal of T1 around the frequency of 0.24 Hz, the characters of the bending and torsion were used. For the torsional modes, the upstream and downstream vibrational components at the same

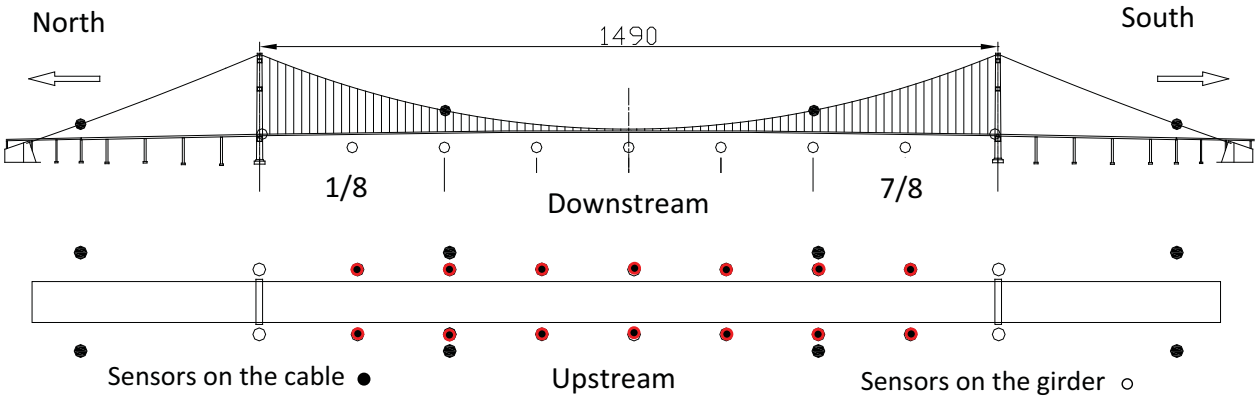

Fig. 2. Layout of accelerometers in SHM system of the RSB.

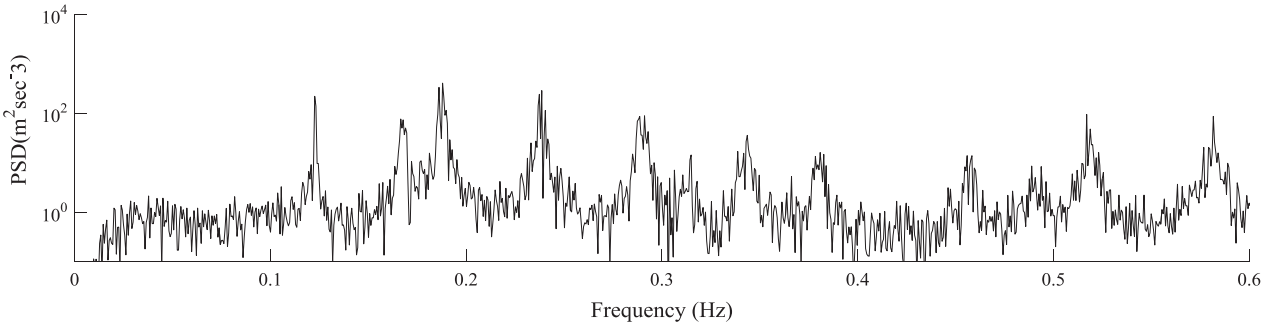

Fig. 3. Power spectral density of deck response at 1/8 section.

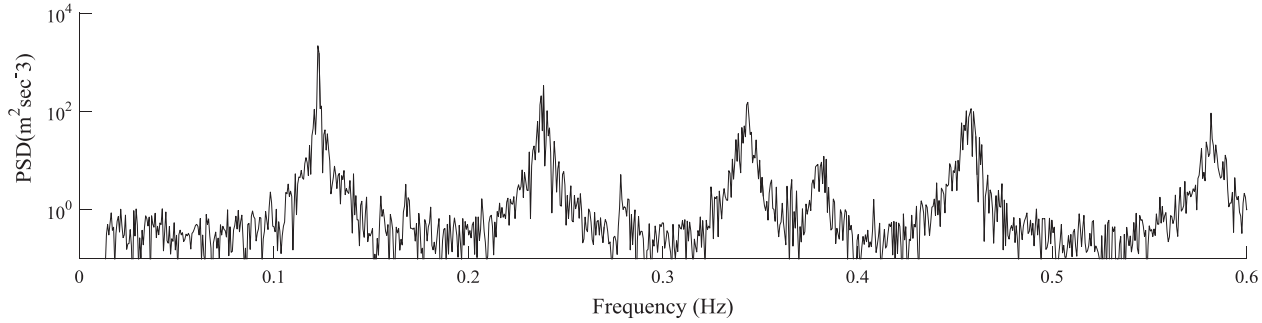

Fig. 4. Power spectral density of deck response at 4/8 section.

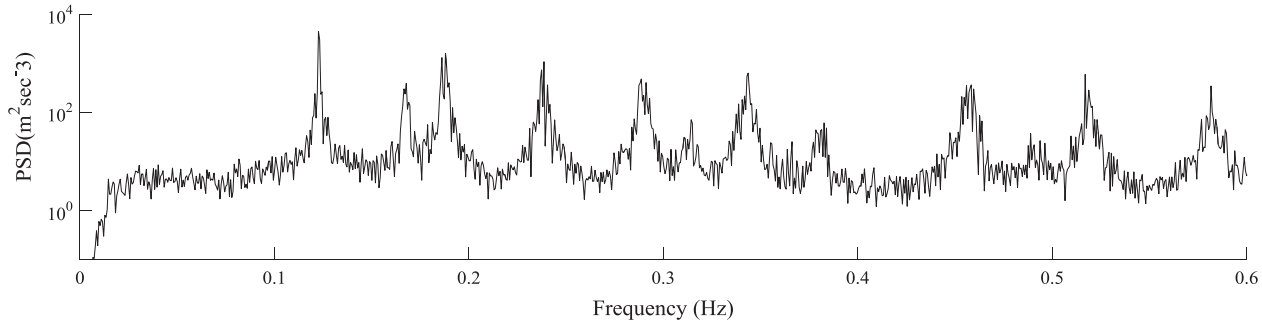

Fig. 5. Trace of PSD ($\boldsymbol{tr}(\boldsymbol{S}_k^{\boldsymbol{sum}})$) of deck responses derived from all measure points.

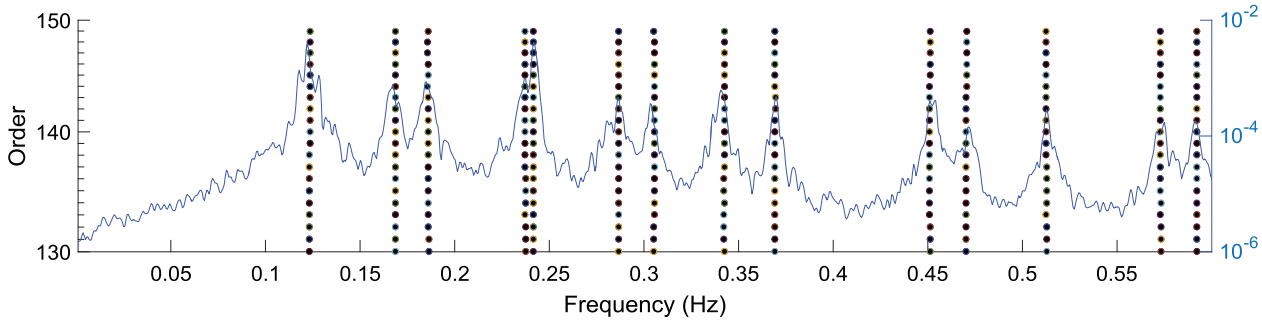

Fig. 6. Stabilization diagram of vertical modes using SSI.

section have opposing phase. When the signals recorded at the upstream and downstream with the same section are added together, the responses related to torsional modes can be eliminated in the new signal. Therefore, the bending response can be separated from the new added vertical response. Similarly, the torsional response can be obtained by subtracting the vertical responses from the simultaneously recorded data at same section. According to this method, the vertical modes and the

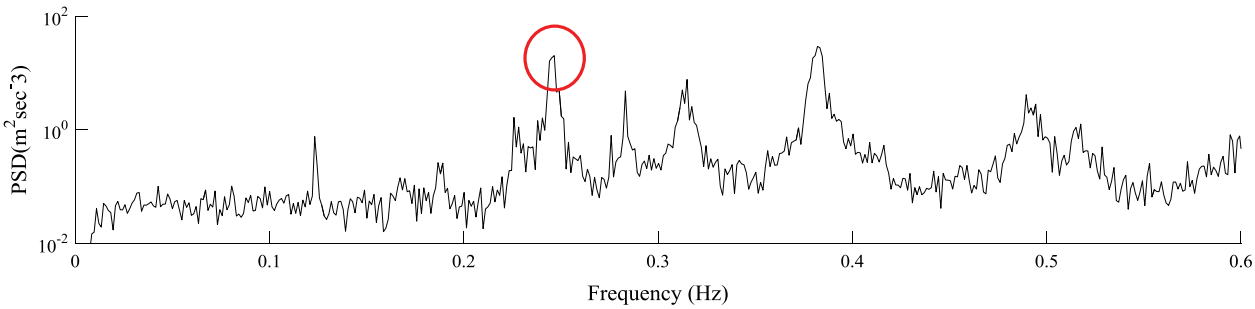

(a) PSD of the torsional mode response

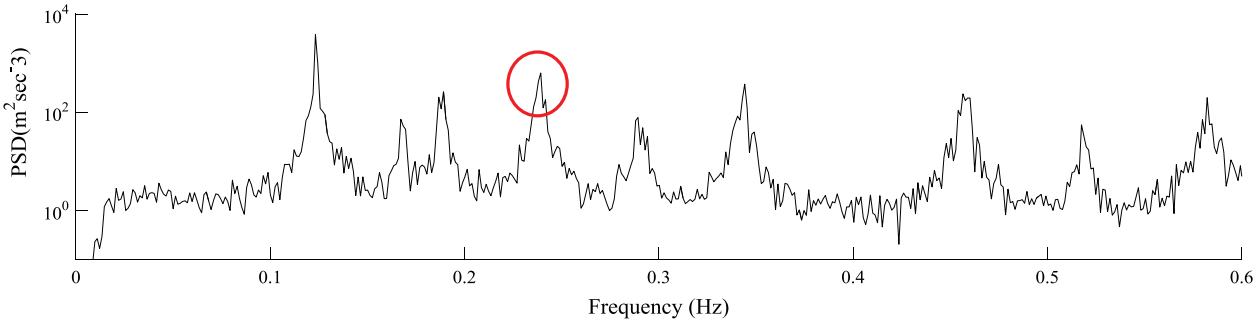

(b) PSD of the bending mode response

Fig. 7. Discrimination of vertical bending and torsional modes.

Table 1
Statistical value of identified modal parameters by the Bayesian method.

Modes	Frequency (Hz)		BSTA Optimal value (MPV)			Coefficient of Variation (C.O.V)		
	FEM	SSI	Frequency (Hz)	Damping (%)	Modal force (N^2/s)	Frequency (%)	Damping (%)	Modal force (%)
V2	0.1250	0.1233	0.1224	0.99	5.9E-2	0.16	8.4	10.8
V3	0.1696	0.1686	0.1675	0.45	7.0E-3	0.13	29.8	26.2
V4	0.1900	0.1865	0.1875	1.07	3.4E-2	0.13	5.9	4.8
V5	0.2418	0.2373	0.2382	0.46	1.6E-2	0.07	20.0	11.2
V6	0.2921	0.2865	0.2892	0.70	1.6E-2	0.10	27.6	25.7
V7	0.3469	0.3423	0.3437	0.75	1.9E-03	0.90	15.5	14.4
T1	0.2383	0.2414	0.2450	0.36	6.0E-04	0.62	25.8	15.5
T2	0.2925	0.3054	0.3114	0.75	1.0E-06	0.07	2.3	9.2
T3	0.3586	0.3692	0.3603	0.46	5.0E-04	0.08	26.6	29.9

torsional modes were successfully separated, as illustrated in Fig. 7. From Fig. 7(a), it can be seen that the frequencies corresponding to first three torsional modes were 0.242 Hz, 0.304 Hz and 0.367 Hz, respectively. From Fig. 7(b), it can be seen the first six bending modes were 0.123 Hz, 0.167 Hz, 0.187 Hz, 0.238 Hz, 0.286 Hz and 0.342 Hz, respectively.

3.5. Statistical results of identified modal parameters

Table 1 summarized the typical identification results of the modal frequencies and damping ratios of the first 9 modes using the Bayesian method. The columns under 'MPV' means most possible value of estimators. The posterior coefficient of variation (C.O.V) is equal to the posterior standard deviation divided by posterior MPV. It was found that the posterior C.O.V is in acceptable range. The C.O.V of all the identified modal frequencies were less than 1.0%. On the other hand, it can be observed that the damping ratios and the modal force have large posterior uncertainty. For these data sets, the damping ratios had a higher C.O.V in the order of a few ten percent. The damping ratios were identified with much higher uncertainty than the natural frequencies.

As far as the frequencies is concerned, the identified results by the SSI method and the calculated results were also presented in Table 1. The SSI method includes two different algorithms: the data-driven (denoted as SSI-DATA) algorithm and the covariance-driven (denoted as SSI-COV) algorithm. In this paper, the SSI-DATA algorithm was applied, which involves the choice of two parameters i_row and i_column. The two parameters are the number of half block rows and the columns of the Hankel matrices, respectively. For the Runyang Suspension bridge, i_row was selected from 130 to 150, and i_column was

given 6000. Comparison of identified results using the Bayesian method and the SSI method, a good agreement can be achieved.

Fig. 8 illustrates the identified mode shapes of two typical modes. Meanwhile, the identified results from a full-scale field test and a finite element model are also presented. Comparison of identified results from the Bayesian method and field test, a good agreement can be achieved.

4. Statistical analysis on long-term extracted results

A long-term modal parameters analysis was performed based on BSTA method using the SHM system data sets over a 3-year period in this bridge's initial life (2005–2007). This section first presents identification of modal parameters based on the vibration data with a duration of one year. Then the effects of the environmental conditions on the model identifications were studied.

4.1. Variation of modal frequency over one-year data sets

Figs. 9–13 show the variations of the five modal frequencies over 1-year (2006) monitoring period. As can be seen in the figures, high variation in the identified modal frequency was observed. This variation is considered due to two reasons. The first reason is the uncertainty introduced in the system in the excitation (e.g., traffic and wind). The second reason for the variation in the identified modal frequencies is known as the environmental effects such as the change in temperature.

The variations of the frequency of mode V2 and V3 were illustrated in Figs. 9 and 10, respectively. It was observed that the identified frequency of the two modes is not sensitive to the temperature. Moreover, the largest standard deviation, associated with the first mode, was only about 2–3%.

Figs. 11–13 present the variation of the identified modal frequency of mode V4, V6 and V7, respectively. The frequency of the modes exhibit fluctuation with the change of the season. It can be seen that there was an obviously decrease in the frequency of higher modes as the temperature increased. Since the minimum temperature usually occurs in January and February, the frequency appears high during that time. In contrast, the modal frequencies decreased as the temperature increased in July and August.

To observe the variability of the confidence intervals for the estimated frequency, the typical posterior coefficient of variations (C.O.V) for the frequency of V3 and V6 are presented in Figs. 14 and 15. It can be seen that the C.O.V of the estimated frequencies exhibit random features.

4.2. Effect of temperature on modal parameters

As mentioned above, it can be seen that some of the identified frequency decreased as the temperature increased. To investigate the influence of the temperature on the model frequency, one typical data sets are provided, which illustrates the relationship between the girder temperature and the modal parameters.

Fig. 16 presents the modal frequency of V7 identified in January 2006. Meanwhile, Fig. 17 presents the corresponding temperature measured by the sensor inside the girder. It can be found that the frequency fluctuates with the change of the temperature. When the temperature changed sharply, such as during the period from January 21 to January 28 (marked in red[1] in Fig. 16), the frequency also exhibited obvious variation. In contrast, when the temperature of the girder varied less gradually (marked in blue in Fig. 16), the modal frequency of V7 appeared to only change slightly. Moreover, the frequency has a negative monotonic relation with the temperature.

For the modal frequencies, fluctuation was observed for all modes. The modal parameters of the RSB exhibit daily and seasonal variation. The changes of some model frequency especially the high order modes were partially due to the variation of ambient temperature.

In addition, it should be noted that the identified modal frequencies using BSTA approach provided an intuitive indication of effects the ambient temperature variations on the changes of the bridge.

4.3. Statistical distribution of modal frequency

Operational modal parameters extracted in the previous section fluctuated with the change of the temperature. Therefore, the mean value of the modal parameters became a good estimation of the system value. The distribution of modal parameters provided information on the uncertainty ranges and the confidence levels. These statistical values are also crucial for advanced structural analysis, such as risk analysis, damage detection, Benchmark model updating. An accurate and reliable statistical model of the modal parameters is crucial for SHM of the large span bridges.

Probability density plots are shown in Figs. 18–21 for four modes V2, V4, V6 and V7, respectively. An hourly observation is used to fit the distributions, which has more than 2500 effective samples. Due to the symmetry of the distributions of the field data, the normal distribution and the t location-scale distribution are separately fitted on the probability density plot of

[1] For interpretation of color in Fig. 16, the reader is referred to the web version of this article.

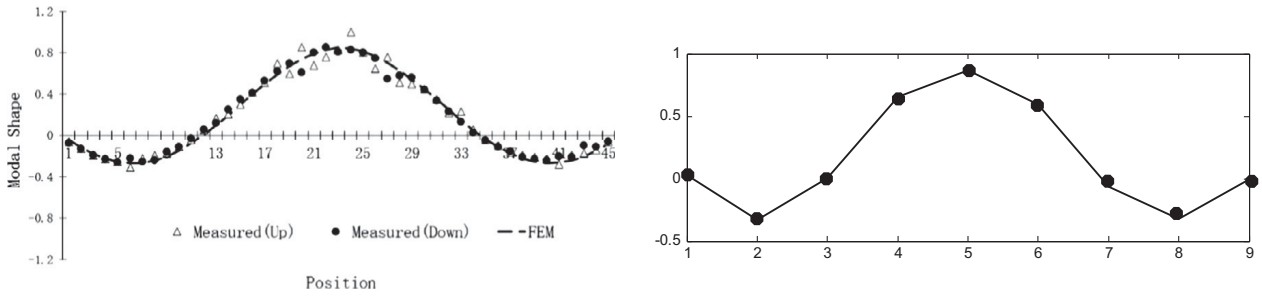

a)1rt symmetric bending mode(V2)

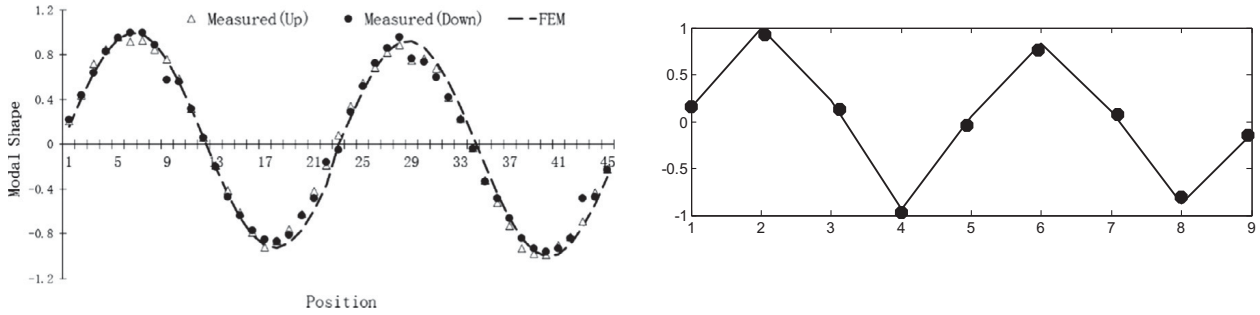

b)2nd anti-symmetric mode(V4)

Fig. 8. Identified vertical mode shapes of the deck.

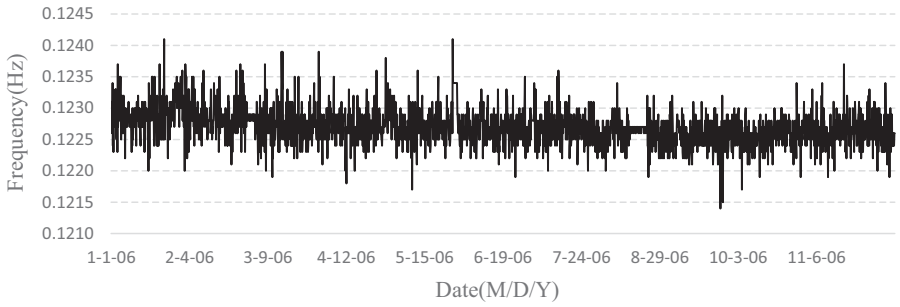

Fig. 9. Variation of the identified modal frequency of V2 in one year.

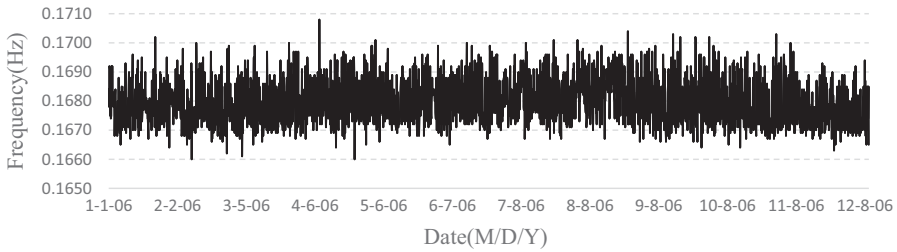

Fig. 10. Variation of the identified modal frequency of V3 in one year.

two lower order modes V2 and V4. It can be seen that the t location-scale distribution was shown to be the better candidate for modal frequency of mode V2 and V4. However, the burr distribution provided a better fit on the mode V6 and V7 than the t location-scale distribution. Environmental influences, such as temperature, have been suspected to be the reason for the dispersion seen in some of higher mode parameters.

Tabel.2 presents the statistical value of the identified modal parameters identified from one-year monitoring. For the first eight modes, the variation of the usual environmental conditions accounted for 2.0–3.0% relative changes in the modal frequencies (see Table 2).

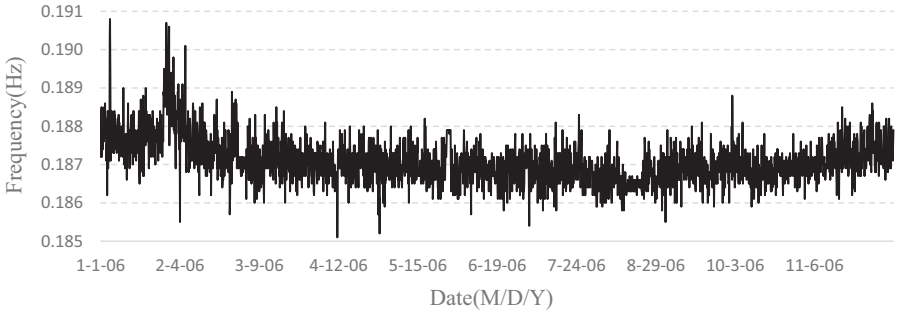

Fig. 11. Variation of the identified modal frequency of V4 in one year.

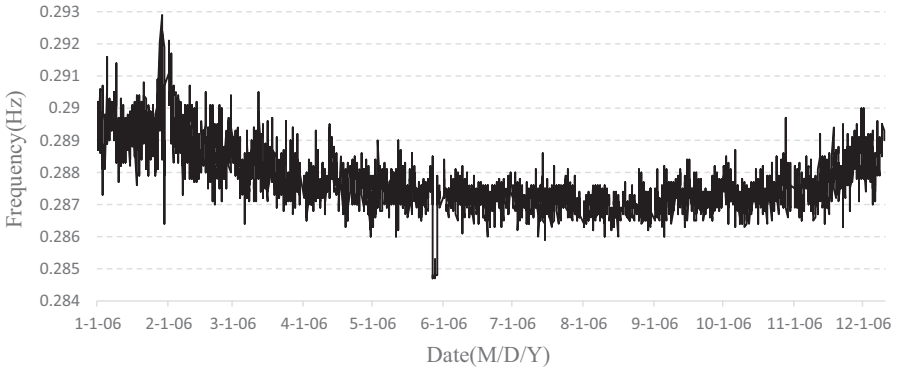

Fig. 12. Variation of the identified modal frequency of V6 in one year.

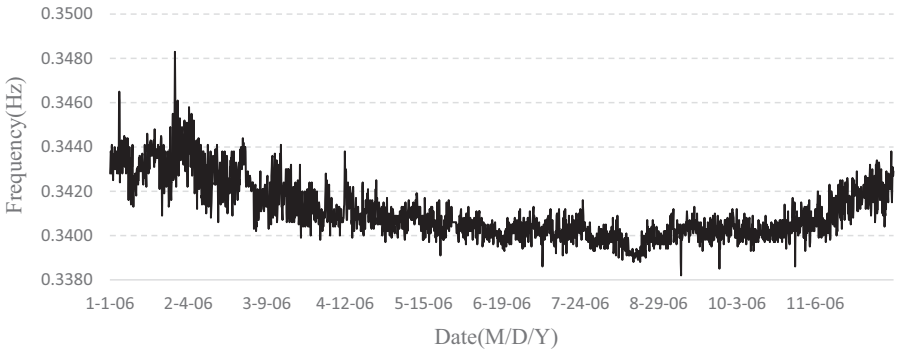

Fig. 13. Variation of the identified modal frequency of V7 in one year.

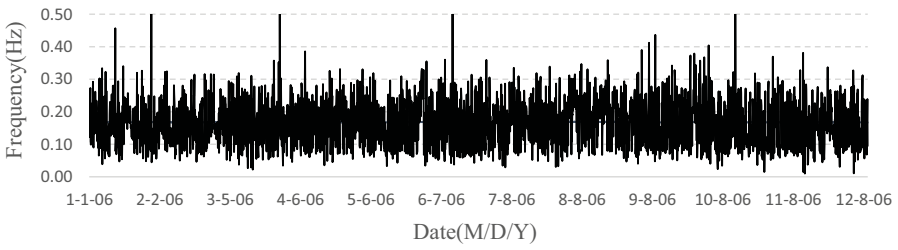

Fig. 14. Variation of the confidence for the identified modal frequency of V3.

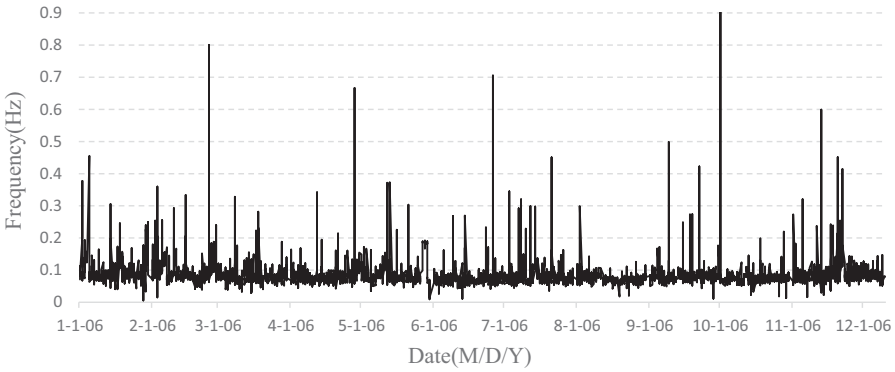

Fig. 15. Variation of the confidence for the identified modal frequency of V6.

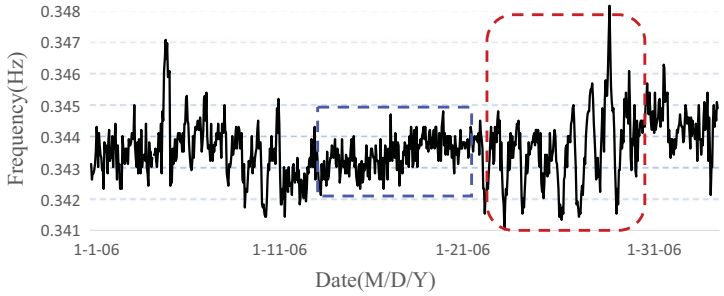

Fig. 16. Variation of the identified modal frequency of V7 in one month.

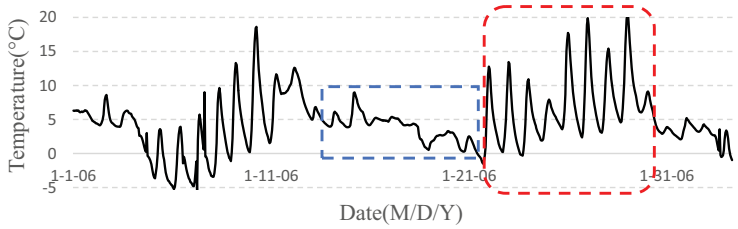

Fig. 17. Variation of the measured temperature in one month.

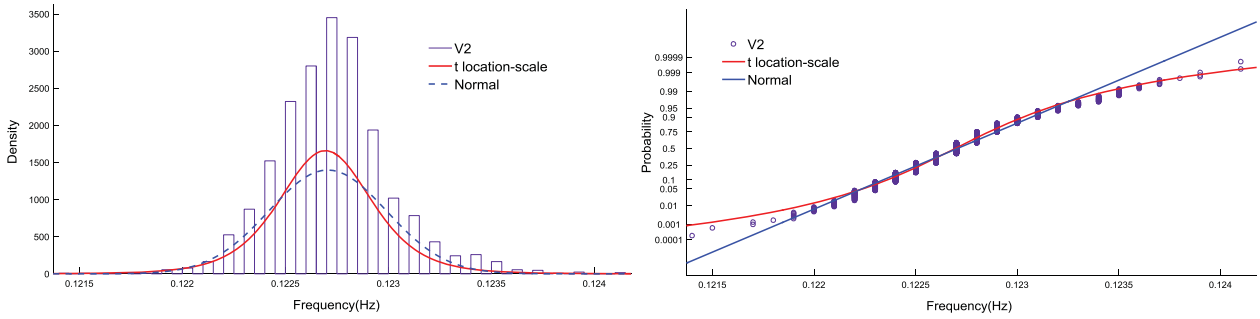

Fig. 18. Statistical distribution of modal frequency of V2.

5. Wind-induced variation of modal parameters

The wind-induced vibration plays an important role for long-span bridges. In wind sensitive slender structures, such as long-span bridges, the model parameters might exhibit significant variations under wind. During the period from August 6 at 16 pm to August 7 at 5 am, 2005, the Typhoon Matsa passed through the Runyang Suspension Bridge. The Typhoon Matsa was the second of eight Pacific tropical cyclones to make landfall on China during the 2005 Pacific typhoon season. When the

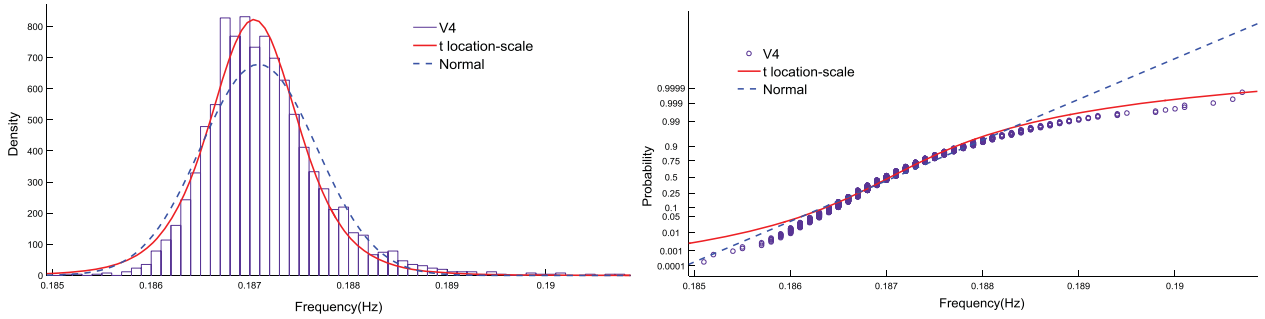

Fig. 19. Statistical distribution of modal frequency of V4.

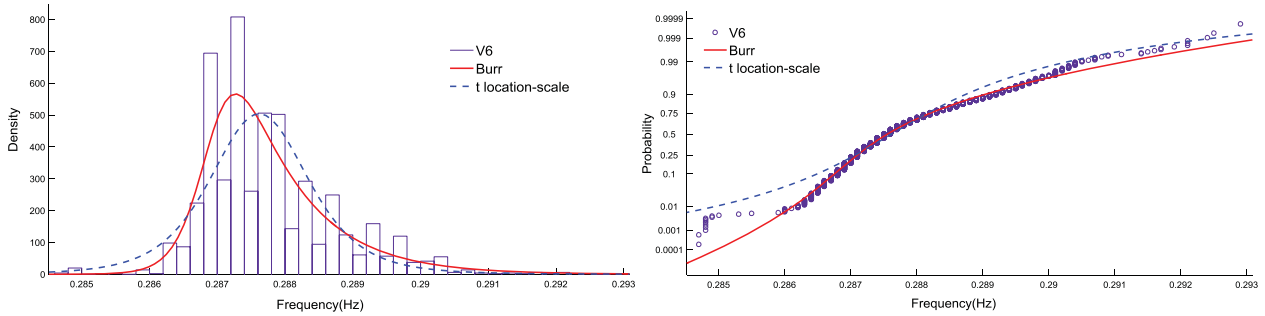

Fig. 20. Statistical distribution of modal frequency of V6.

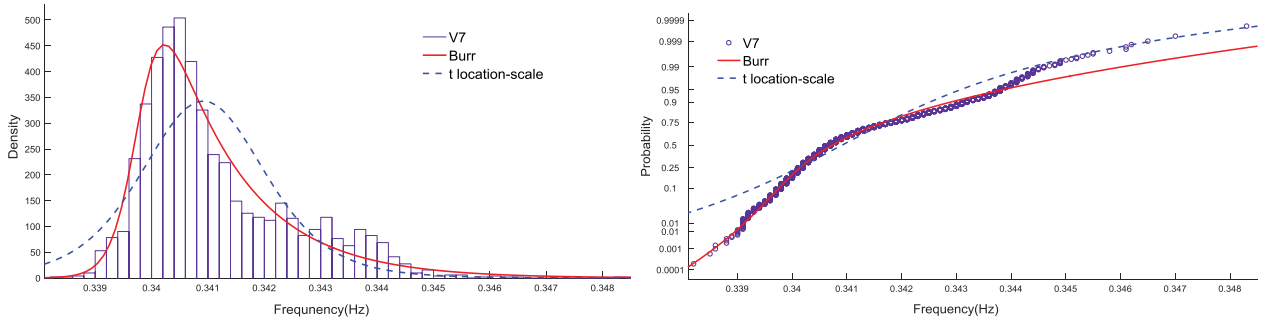

Fig. 21. Statistical distribution of modal frequency of V7.

Table 2
Statistical value of identified modal parameters during one-year monitoring.

Number	Mode	Frequency (Hz)			Relative variation (%)
		Maximum	Minimum	Average	
1	V2	0.1241	0.1214	0.1227	2.2
2	V3	0.1708	0.1660	0.1680	2.9
3	V4	0.1907	0.1851	0.1871	3.0
4	V6	0.2929	0.2847	0.2878	2.8
5	V7	0.3483	0.3382	0.3411	3.0

strong wind passed through the bridge, the mean wind speed value in the whole analysis period was 11.6 m/s and the maximum 1-min mean wind speed reached 20.0 m/s.

Fig. 22 presented the wind speed at the center of the girder during the period from August 6 to August 11. Fig. 23 presented the vertical displacement of the deck recorded by the GPS during the period from August 5 to August 14, 2005. Meantime, the corresponding temperature inside the girder box was also presented in Fig. 24.

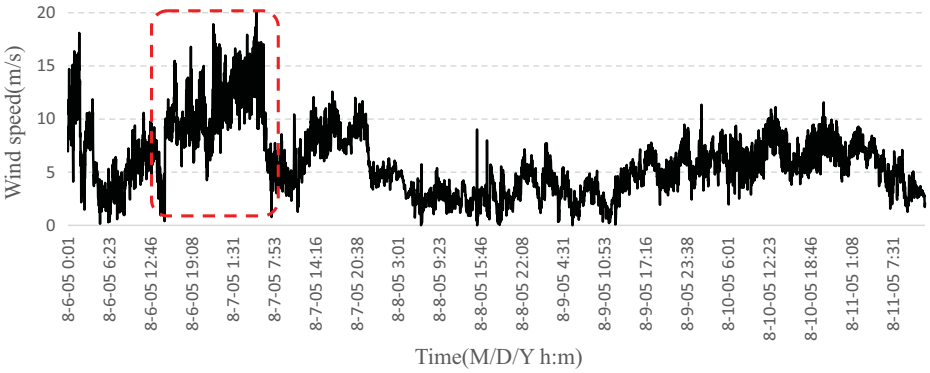

Fig. 22. Wind speed recorded at the center of the girder.

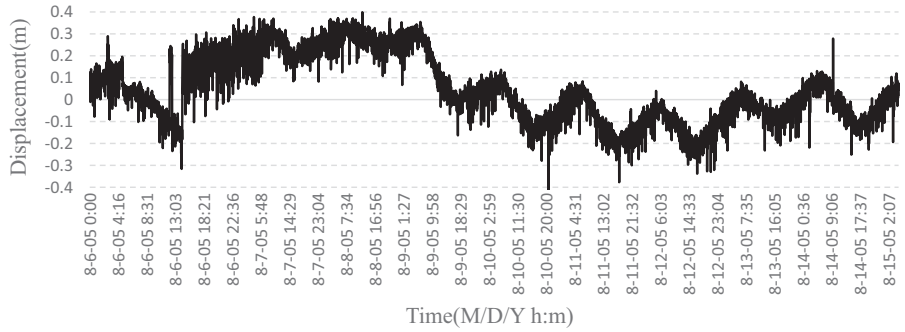

Fig. 23. Vertical displacement of the deck recorded by GPS.

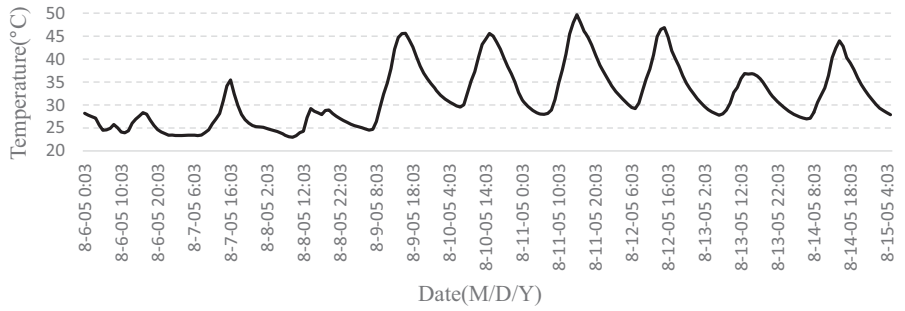

Fig. 24. Temperature of the girder measured from August 6 to August 15, 2005.

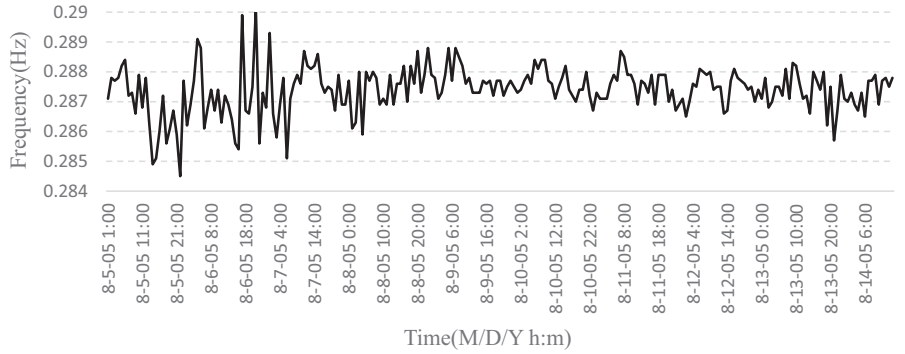

Fig. 25. Variation of the identified modal frequency of V6 during the strong wind period.

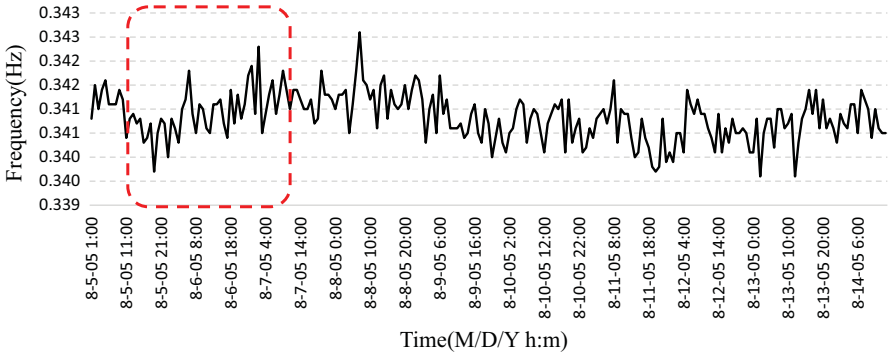

Fig. 26. Variation of the identified modal frequency of V7 during the strong wind period.

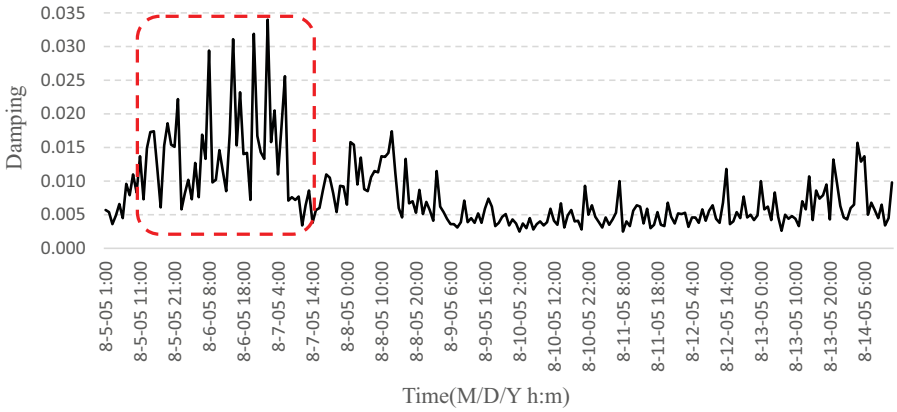

Fig. 27. Variation of the identified modal damping of V6 during the strong wind period.

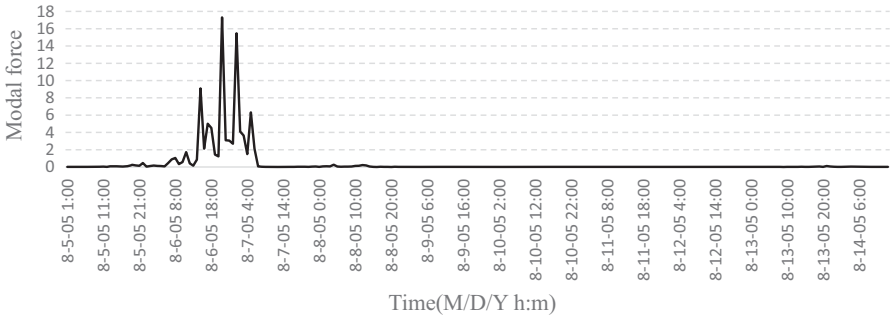

Fig. 28. Variation of the identified modal force of V6 during the strong wind period.

5.1. Effect of wind on modal frequency

Figs. 25 and 26 show the variation of frequency for mode V6 and V7 identified from August 5 to August 14, 2005. It can be observed that variance of the frequency of modes V6 fluctuate significantly during strong wind excitation, compared with that in normal wind condition. However, there is no obvious change in the variance of mode V7.

The fluctuation of modal frequency can be decomposed into regular and irregular components. The regular element is mainly attributed to temperature influence, which exhibits seasonal variation. The irregular element is due to random load, including wind and traffic. During the period of typhoon excitation, the bridge was closed to traffic. Therefore, only the temperature and wind effects account for the fluctuation in the duration of typhoon excited. To distinguish between trend and random elements of fluctuation, the variation of temperature of the deck during the same period is also presented, as shown in Fig. 24. Comparison of the variation of displacement, as shown in Fig. 23, with the variation of the temperature shows that the change of the vertical displacement of the deck correlate well with the change of the temperature. It indicates that thermal effects on bridge vertical deformation appeared to be the strongest environmental influence on bridge behavior, and it is

highly likely that this deformation can lead to secondary effects on the cable tension and even, through nonlinear effects, on modal frequencies.

5.2. Effect of wind on modal damping

Figs. 27 and 28 show the modal damping and modal force of mode V6 identified from August 5 to August 14, 2005. It can be seen that the damping increased when the typhoon was excited, as shown in the period from August 5, 16:00 to August 7, 5:00. Meanwhile, as can be illustrated that the modal force increased sharply when the Typhoon passed through the bridge. It can be observed that the modal damping ratios exhibited significant correlation with the corresponding modal forcing spectral intensities. In addition, it is worth notice that other vertical damping exhibits the similar variation as the mode of V6.

6. Conclusions

In this paper, a Bayesian spectral density method was successfully applied to identify modal parameters of a long-span suspension bridge based on its large sensor data sets. There are two main sources of uncertainty in the identification problem treated, which are due to the estimation and the variable environmental and operational conditions. The first uncertainty can be quantified by the BSTA. The second uncertainty was treated by the statistical method. Through Bayesian inference, not only the modal parameters but also their uncertainties were estimated. Statistical studies were performed on the extracted bridge modal parameters to quantify their distributions and to model their relationships with the environment parameters. The following conclusions are drawn from the study:

(1) The Bayesian spectral method is effective in finding the exact solution of the most possible values of the modal parameters and their posterior coefficients of variation. The posterior coefficient of variation of frequencies are less than 1%. However, the damping ratios were identified with much higher uncertainty than the natural frequencies. Based on the coefficient of variation, the extraction of modal parameters was fully automated.
(2) The Bayesian spectral method is sensitive enough to reveal fluctuations in frequencies of all the modes including high-frequency modes. Results show that the extracted modal parameters of the suspension bridge exhibit daily and seasonal variations. Thermal appeared to be the most significant effects on the frequency of some high order modes. Meanwhile, the bridge vertical deformation exhibited significant correlation with the temperature. The configuration of the bridge can lead to secondary effects on modal frequencies.
(3) Statistical studies were performed to successfully model the statistical distribution of the model frequencies of the long-span suspension bridge, using a large amount of sensor data collected over a one-year period. A t location-scale distribution was found to be an excellent candidate function for the first two lower order modes, i.e., V2 and V3, which were not sensitive to temperature. On the other hand, a burr distribution was shown to be appropriate for modeling the higher modes that are sensitive to temperature influence.
(4) Wind-induced variation in the modal parameters was investigated. It was observed that both the damping ratios and modal forces increased during the Typhoon-induced high-wind excitations. The modal damping ratios exhibited significant correlation with the corresponding modal forcing spectral intensities.

Acknowledgements

The authors would like to express thanks to Professor Aiqun Li and Professor Xiaolin Han of Southeast University and to Professor Wangan Zheng of the AZCRAS company. This study was funded by the National Natural Science Foundation of China (Grant Number 51208252) and the National Key Basic Research Program of China (Grant No. 2013CB036300).

References

[1] H. Sun, D.M. Feng, Y. Liu, M.Q. Feng, Statistical regularization for identification of structural parameters and external loadings using state space models, Comput.-Aided Civ. Infrastruct. Eng. 30 (11) (2015) 843–858.
[2] H. Sohn, Effects of environmental and operational variability on structural health monitoring, Philos. Trans. R. Soc. A-Math. Phys. Eng. Sci. 365 (1851) (2007) 539–560.
[3] J.M. Ko, Y.Q. Ni, Technology developments in structural health monitoring of large-scale bridges, Eng. Struct. 27 (12) (2005) 1715–1725.
[4] Z.J. Li, A.Q. Li, J.A. Zhang, Effect of boundary conditions on modal parameters of the Run Yang Suspension Bridge, Smart Struct. Syst. 6 (8) (2010) 905–920.
[5] A. Cunha, E. Caetano, F. Magalhaes, C. Moutinho, Recent perspectives in dynamic testing and monitoring of bridges, Struct. Control Health Monitoring 20 (6) (2013) 853–877.
[6] B. Peeters, G. De Roeck, Stochastic system identification for operational modal analysis: a review, J. Dyn. Syst. Measur. Control-Trans. ASME 123 (4) (2001) 659–667.
[7] E.P. Carden, A. Mita, Challenges in developing confidence intervals on modal parameters estimated for large civil infrastructure with stochastic subspace identification, Struct. Control Health Monitoring 18 (1) (2011) 53–78.
[8] S.C. Kuok, K.V. Yuen, Structural health monitoring of Canton Tower using Bayesian framework, Smart Struct. Syst. 10 (4–5) (2012) 375–391, Oct-Nov 2012.

[9] L.S. Katafygiotis, K.V. Yuen, Bayesian spectral density approach for modal updating using ambient data, Earthq. Eng. Struct. Dyn. 30 (8) (2001) 1103–1123.
[10] F.T.K. Au et al, Simulation of vibrations of Ting Kau Bridge due to vehicular loading from measurements, Struct. Eng. Mech. 40 (4) (2011) 471–488.
[11] W.-J. Yan, L.S. Katafygiotis, A two-stage fast Bayesian spectral density approach for ambient modal analysis. Part I: posterior most probable value and uncertainty, Mech. Syst. Signal Process. 54–55 (March) (2015) 139–155.
[12] W.-J. Yan, L.S. Katafygiotis, A two-stage fast Bayesian spectral density approach for ambient modal analysis. Part II: mode shape assembly and case studies, Mech. Syst. Signal Process. 54–55 (March) (2015) 156–171.
[13] S.K. Au, F.L. Zhang, Y.C. Ni, Bayesian operational modal analysis: theory, computation, practice, Comput. Struct. 126 (September) (2013) 3–14.
[14] Y.Q. Ni, Y. Xia, W.Y. Liao, J.M. Ko, Technology innovation in developing the structural health monitoring system for Guangzhou New TV Tower, Struct. Control Health Monitoring 16 (1) (2009) 73–98.
[15] Y.L. Ding, A.Q. Li, Temperature-induced variations of measured modal frequencies of steel box girder for a long-span suspension bridge, Int. J. Steel Struct. 11 (2) (2011) 145–155.
[16] H.C. Gomez, P.J. Fanning, M.Q. Feng, S. Lee, Testing and long-term monitoring of a curved concrete box girder bridge, Eng. Struct. 33 (10) (2011) 2861–2869.
[17] H.C. Gomez, H.S. Ulusoy, M.Q. Feng, Variation of modal parameters of a highway bridge extracted from six earthquake records, Earthq. Eng. Struct. Dyn. 42 (4) (2013) 565–579.
[18] J.M.W. Brownjohn, F. Magalhaes, E. Caetano, A. Cunha, Ambient vibration re-testing and operational modal analysis of the Humber Bridge, Eng. Struct. 32 (8) (2010) 2003–2018.
[19] D.M. Siringoringo, Y. Fujino, System identification of suspension bridge from ambient vibration response, Eng. Struct. 30 (2) (2008) 462–477.
[20] F.N. Catbas, M. Susoy, D.M. Frangopol, Structural health monitoring and reliability estimation: long span truss bridge application with environmental monitoring data, Eng. Struct. 30 (9) (2008) 2347–2359.
[21] K.V. Yuen, L.S. Katafygiotis, J.L. Beck, Spectral density estimation of stochastic vector processes, Probab. Eng. Mech. 17 (3) (2002) 265–272.
[22] H. Wang, A. Li, T. Guo, T. Tao, Establishment and application of the wind and structural health monitoring system for the Runyang Yangtze River bridge, Shock Vib. (2014) 421038.